randomly selected workers were individually marked with colored, numbered plastic tags. One hundred tagged bees were treated topically with 200 μg of (*RS*)-methoprene (isopropyl (2*E*, 4*E*)-11-methoxy-3,7,11-trimethyl-2,4-dodecadienoate) dissolved in 5 μl of acetone, and 100 were treated with acetone alone. Although recent evidence [G. D. Prestwich, *Science* **237**, 999 (1987)] suggests that there are different receptor sites for JH homologs and analogs in the tissue of at least one insect species (*Manduca sexta*), methoprene has demonstrated JH-like activity in many species, at the molecular [G. R. Wyatt, K. E. Cook, H. Firko, T. S. Dhadialla, *Insect Biochem.* **17**, 1071 (1987)], physiological, and behavioral levels [G. B. Staal, *Annu. Rev. Entomol.* **20**, 417 (1975)]. The efficacy of methoprene as a JH analog in honey bees is well established (*15, 16*). We quantified the incidence of precocious foraging among the two groups of tagged bees during daily 1-hour observation periods at the colony entrance, when bees were 5 to 10 days old. A census of tagged bees was also taken early in the morning of day 11, before the onset of foraging.

25. H. Sasagawa, *Honeybee Sci.* **10**, 65 (1989).
26. R. Feyereisen, *Comprehensive Insect Physiology Biochemistry and Pharmacology*, G. A. Kerkut and L. I. Gilbert, Eds. (Pergamon, Oxford, 1985), vol. 7, pp. 391–429; S. S. Tobe and B. Stay, *Adv. Insect Physiol.* **18**, 305 (1985).
27. S. Taber and J. Wendel, *J. Econ. Entomol.* **51**, 786 (1958).
28. J. Adams, E. D. Rothman, W. E. Kerr, Z. L. Paulino, *Genetics* **86**, 583 (1977).
29. R. E. Page and R. A. Metcalf, *Am. Nat.* **119**, 263 (1982).
30. H. H. Laidlaw and R. E. Page, *Genetics* **108**, 985 (1984).
31. Allozymes of malate dehydrogenase-1 (*Mdh*) that occur naturally in populations of honey bees (*29*) were used as subfamily markers, as in (*9*). Three unrelated virgin queens were instrumentally inseminated [H. H. Laidlaw, *Instrumental Insemination of Honey Bee Queens* (Dadant and Sons, Hamilton, IL, 1977)] with the semen of three unrelated drones. Each drone carried a different *Mdh* allozyme, designated "slow" (S), "medium" (M), and "fast" (F) [E. P. B. Contel, M. A. Mestriner, E. Martins, *Biochem. Genet.* **15**, 859 (1977)]. Three single-cohort colonies were established (*18*) from the progeny of each queen. Use of allozyme markers allowed blind behavioral observations. Individuals sampled for JH titer determinations were among those used for allozyme analysis (with polyacrylamide gel electrophoresis).
32. N. W. Calderone, G. E. Robinson, R. E. Page, *Experientia*, in press.
33. J. T. Bonner, *The Evolution of Complexity by Means of Natural Selection* (Princeton Univ. Press, Princeton, NJ, 1988).
34. R. R. Sokal and F. J. Rohlf, *Biometry* (Freeman, San Francisco, ed. 2, 1981).
35. We thank I. Muller for translating articles, O. R. Taylor for providing pheromone swarm lures, G. B. Staal for providing methoprene, J. R. Bart, N. W. Calderone, J. P. Delbecque, M. K. Fondrk, and J. A. Gianelos for assistance, H. H. Hagedorn for discussion, and D. L. Denlinger, J. F. Downhower, R. Nowogrodzki, T. D. Seeley, W. R. Tschinkel, and M. J. West-Eberhard for reviewing the manuscript. Supported by postdoctoral fellowships from NSF (BSR-8800227) and The Ohio State University (G.E.R.), NSF grant BNS-8719283 (R.E.P.), and the CNRS (C.S. and A.S.).

9 May 1989; accepted 15 August 1989

Dispersed Polaron Simulations of Electron Transfer in Photosynthetic Reaction Centers

A. WARSHEL,* Z. T. CHU, W. W. PARSON

A microscopic method for simulating quantum mechanical, nuclear tunneling effects in biological electron transfer reactions is presented and applied to several electron transfer steps in photosynthetic bacterial reaction centers. In this "dispersed polaron" method the fluctuations of the protein and the electron carriers are projected as effective normal modes onto an appropriate reaction coordinate and used to evaluate the quantum mechanical rate constant. The simulations, based on the crystallographic structure of the reaction center from *Rhodopseudomonas viridis*, focus on electron transfer from a bacteriopheophytin to a quinone and the subsequent back-reaction. The rates of both of these reactions are almost independent of temperature or even increase with decreasing temperature. The simulations reproduce this unusual temperature dependence in a qualitative way, without the use of adjustable parameters for the protein's Franck-Condon factors. The observed dependence of the back-reaction on the free energy of the reaction also is reproduced, including the special behavior in the "inverted region."

THE RECENT ELUCIDATION OF THE crystal structure of photosynthetic bacterial reaction centers (*1–3*) has made it possible to explore microscopic aspects of biological electron transfer (ET) theory. Although a semiclassical trajectory simulation of the initial ET reaction has been reported (*4*), no attempts have been made to use a microscopic simulation approach to account for the unusual temperature dependence of the ET reactions or to treat nuclear tunneling effects. We report such a study for the charge-transfer step $P^+H^-Q \rightarrow P^+HQ^-$, where P is the primary electron donor in the reaction center (a bacteriochlorophyll dimer), H is a bacteriopheophytin that accepts an electron from P when the reaction center is excited, and Q is the secondary electron acceptor (ubiquinone in *Rhodobacter sphaeroides* or menaquinone in *Rhodopseudomonas viridis*). We also have studied some aspects of the slower back-reaction $P^+HQ^- \rightarrow PHQ$.

The kinetics of the ET reaction $P^+H^-Q \rightarrow P^+HQ^-$ and of the reaction from Q^- back to P^+ have been measured over a wide range of temperatures (*5–9*). In *Rb. sphaeroides*, both reactions are characterized by an intriguing decrease in rate constant with increasing temperature. In *Rps. viridis*, the rates are almost independent of temperature. The dependence of the kinetics on the free energies of the reactions also has been studied, by varying the nature of the quinone or by applying external electrical fields (*7–9*). The back-reaction is particularly interesting in this regard, because the change in free energy is so large as to place the reaction in the "inverted region" (*10–12*) where the rate constant depends strongly on quantum mechanical (QM) nuclear tunneling.

Previous discussions of the dependence of the rate constants on temperature or on the free energy change have consisted largely of fitting the data to theoretical expressions with adjustable phenomenological parameters (*10*). Although these treatments have provided considerable insight into the factors that influence electron reactions in proteins,they have not been based on the actual structure of the protein. Thus, it has been possible to fit the experimental data in different ways by making various assumptions about the type and numbers of vibrational modes that are coupled to the reaction. The availability of the crystal structure makes it possible to evaluate the key parameters directly from the structure by using microscopic simulations.

In the present work we examine the above reactions, using the "dispersed polaron" version (*13, 14*) of our semiclassical trajectory approach (*4, 12, 13*). The dispersed polaron method extends the semiclassical surface-crossing method to the evaluation of QM tunneling effects. Thus we can simulate the temperature dependence of the rate constants and the special behavior in the inverted region, using the actual microscopic properties of the protein and the chromophores.

Electron transfer between a weakly interacting donor and acceptor (such as H^- and Q) can occur only when the potential energy surfaces of the reactant and product states

A. Warshel and Z. T. Chu, Department of Chemistry, University of Southern California, Los Angeles, CA 90007.
W. W. Parson, Department of Biochemistry, University of Washington, Seattle, WA 98195.

*To whom correspondence should be addressed.

intersect. Thus one can obtain the rate constant for an ET reaction by running classical molecular dynamics (MD) trajectories on the reactant potential surface (V_a) and counting a transition to the product surface (V_b) each time $\Delta V_{ba}(t) = V_b - V_a = 0$, with a probability factor P_{ab} so that (*12, 13*)

$$k_{ab} = \Sigma_{\text{crossings}} P_{ab}(\tau_i)/\tau \quad (1)$$

where

$$P_{ab}(\tau_i) = |(\sigma_{ab}/\hbar)$$

$$\int_{\tau_i - \delta}^{\tau_i + \delta} \exp[-(1/\hbar) \int_0^t \Delta V_{ba}(t')dt']dt|^2_{V_a}$$

Here σ_{ab} is the Hamiltonian matrix element that describes the electronic interaction between the wave functions of states a and b, $\hbar$ is Planck's constant, τ_i is the time of the ith crossing, τ is the total time, and the subscript V_a designates evaluation of ΔV with trajectories that are propagated over

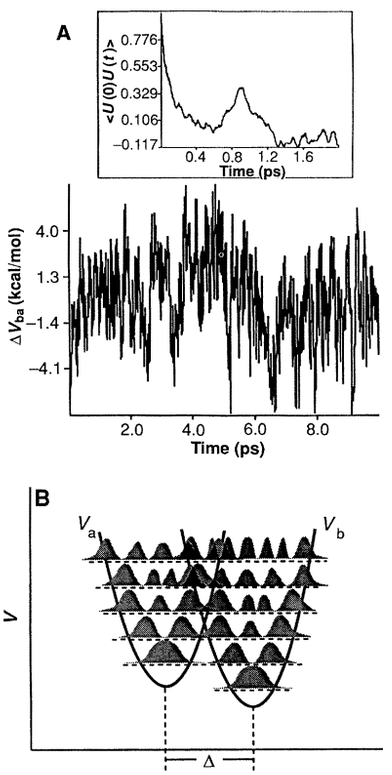

Fig. 1. (**A**) The time-dependent energy gap $\Delta V(t)$ for the charge-transfer reaction $H^-Q \rightarrow HQ^-$, as calculated during a trajectory on the potential surface H^-Q. The ET reaction has a significant probability whenever $\Delta V(t)$ is zero. The inset shows the autocorrelation of $U(t)$, where $U(t)$ is the difference between $\Delta V(t)$ and the average of $\Delta V(t)$. (**B**) Schematic description of nuclear tunneling between the vibrational wave functions of the reactant and product surfaces (V_a and V_b, respectively). The shaded areas represent the squares of the amplitudes of the vibrational wave functions. Electron transfer can occur when the two wave functions overlap.

V_a. In most cases, P_{ab} reduces to the well-known Landau-Zener factor, which describes the probability of hopping between weakly coupled potential surfaces (*13*). Thus we can evaluate the corresponding $\Delta V_{ba}(t)$ as a function of time t (Fig. 1A) and obtain the rate constant through Eq. 1. This semiclassical expression is formally equivalent in the high-temperature limit (*13*) to the familiar Marcus expression (*15*) but can reflect the energetics and fluctuations of the actual microenvironment in a complex system such as a protein.

The above approach is very useful for ET simulations at moderate temperature (*4*), and even qualitative monitoring of $\Delta V(t)$ can be instructive (*12, 16*). However, in treating low-temperature ET one must also consider nuclear tunneling, which allows ET to occur even when the classical potential surfaces V_a and V_b do not intersect. The problem can be formulated in terms of the integrals of the QM vibrational wave functions for the reactant and product states (the squares of these integrals are the Franck-Condon factors). In general, the vibrational wave functions of states a and b always have nonzero overlap (see Fig. 1B). This overlap provides a finite probability that the system will tunnel from state a to state b even at zero temperature, when classical motion does not allow the vibrating nuclei to reach a point where $V_a = V_b$. As will be shown below, one can obtain approximate values of the relevant overlap parameters for the protein by using a Fourier transform of the same high-temperature energy gap, $\Delta V_{ba}(t)$, that was used in Eq. 1.

The QM rate constant for a multidimensional harmonic system is given by (*17*)

$$k_{a \rightarrow b} = |\sigma_{ab}/\hbar|^2 \int_{-\infty}^{\infty} \exp[i\omega_{ba}t + \gamma(t)]dt \quad (2)$$

where $\omega_{ba} = \langle V_{ba} \rangle_a / \hbar$ and $\langle \ \rangle_a$ designates an average over trajectories on V_a. The quantity $\gamma(t)$ is the QM correlation function,

$$[\gamma(t) = \sum_j \Delta_j^2[(\bar{n}_j + 1/2)(\cos \omega_j t - 1) + i\sum_i (\Delta_j^2/2)\sin \omega_j t)] \quad (3)$$

where Δ_j and ω_j are, respectively, the dimensionless coordinate displacement (origin shift) and frequency of the jth normal vibrational mode (ω_j is assumed to be the same in state a and state b); $\bar{n}_j$ is given by

$$\bar{n}_j = [\exp(\hbar\omega_j/k_b T) - 1]^{-1}$$

where k_b is the Boltzmann constant and T is the temperature. The parameters Δ_j determine the overlap between the QM wave functions for the nuclear vibrations in states a and b.

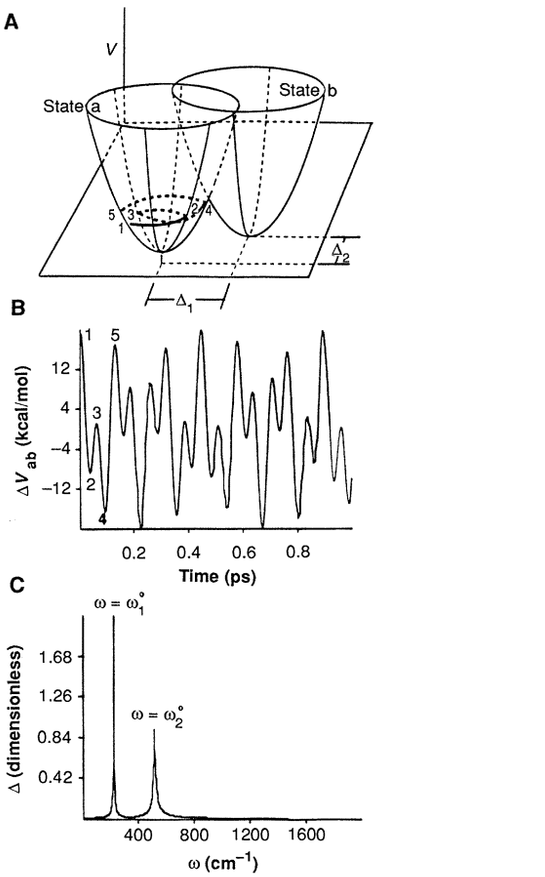

Fig. 2. (**A**) Schematic description of the relation between the oscillations of a trajectory on state a for a two-dimensional harmonic system; Δ_1 and Δ_2 are the two components of the displacement vector connecting the minima of the two potential surfaces. (**B**) The corresponding time dependence of the energy gap between states b and a, ΔV_{ab}. (**C**) The Fourier transform of ΔV_{ab}.

Equation 2 provides a direct prescription for calculating the temperature dependence of the rate constant through the temperature dependence of the $\bar{n}$ values. Rather than evaluating the integral in Eq. 2 directly, it generally is necessary to use an analytical continuation of this equation, which can be obtained by expanding the exponential term in t (*13*). However, any realistic molecular calculation requires the origin shifts Δ_j associated with the protein vibrations, and these parameters are not available from direct experimental information. Fortunately, the time dependence of the energy gap $\Delta V_{ba}(t)$ of Fig. 1 contains the information needed for the evaluation of the Δ_j and ω_j values. To see this, consider the two-dimensional harmonic system shown in Fig. 2, A and B. When the system is at the turning points on the left (such as point 1), ΔV_{ba} will reach its largest values; at turning points on the right (such as point 2), ΔV_{ba} will be at a minimum. The frequencies of the oscillations of ΔV_{ba} are determined by the curvature of V_a, and the amplitudes of these oscillations de-

pend on Δ_1 and Δ_2 (the horizontal displacements of the minima of V_a and V_b with respect to coordinates 1 and 2). The larger the displacements, the larger the amplitudes. If both displacements are zero, the oscillations of ΔV_{ba} will have zero amplitude.

A Fourier transform of the ΔV_{ba} shown in Fig. 2B gives two peaks at frequencies ω_1 and ω_2 with heights proportional to Δ_1 and Δ_2 (Fig. 2C). For surfaces with more dimensions, the oscillations of $\Delta V_{ba}(t)$ will reflect a variety of motions with different frequencies and different displacements. A Fourier transform of the energy gap for two n-dimensional surfaces projects the energy gap on the n coordinates and gives the one-dimensional equivalent of Fig. 2 for each mode.

A procedure for evaluating the multidimensional Δ_j and ω_j parameters from $\Delta V_{ba}(t)$ has been described in detail elsewhere (*13*). A simple Fourier transform of the ΔV_{ba} obtained from classical trajectories on V_a can thus provide the Δ and ω parameters for the low-temperature harmonic rate constant. Although the vibrations of a protein can be highly anharmonic, the Fourier transform procedure allows one to model a complex system of this sort by relating the relevant fluctuations to those of a multidimensional harmonic system with the same power spectrum (*18*). This procedure requires one to normalize the Δ_j values through the relation (*13, 18, 19*)

$$\frac{1}{2}\sum_i \omega_i \Delta_i^2 = \lambda = \langle \Delta V_{ba} \rangle_a - \Delta G^0 \quad (4)$$

where λ is the so-called reorganization energy and ΔG^0 is the free energy of the reaction. The evaluation of these key parameters will be considered below.

Explicit potential surfaces for the particular system under study can be obtained from the force fields (*4, 20*)

$$V_i = V_{protein} + V^i_{strain} + V^i_{elec} + \alpha^i \quad (5)$$

Here $V_{protein}$ represents the force field of the protein-protein and water-protein interactions, and V^i_{strain} is the intramolecular force field of the donor (D) and acceptor (A) molecules in electronic state i; V^i_{elec} represents the intermolecular electrostatic interactions between D and A in state i and also the interaction of the atoms of these two molecules with the rest of the protein-water system, including the effects of the protein residual charges, nearby water molecules, and the induced dipoles in the protein. The term α^i is the intramolecular gas-phase free energy of the electron carriers in state i, at infinite separation between the D and A species, relative to the corresponding energy in the ground state.

The quantities ΔG^0 and λ can be evaluated from the potential (Eq. 5) by a free energy perturbation method (*4, 12*), which uses a mapping potential of the form

$$V_m = V_a(1 - \theta_m) + V_b\theta_m \quad (6)$$

The mapping potential drives the system from the reactant to the product state in ten simulation steps of 2-ps each, with equal increments of θ_m between 0 and 1. This process allows the protein and the electron carriers to relax in response to the new charges and provides a projection of the free energy surfaces of states a and b on the optimal reaction coordinate (*13*). The resulting free energy functionals, Δg_a and Δg_b (Fig. 3A), are closely related to the parabolic curves in Marcus's (*15*) classical treatment of ET reactions [see (*12*) for discussion], but the present procedure obtains these curves for a biological D and A by using the actual protein coordinates and realistic interatomic forces. The values of ΔG^0 and λ obtained for the $H^-Q \rightarrow HQ^-$ reaction were approximately 11 and 13 kcal/mol, respectively. The free energy functionals obtained from the microscopic simulation are not exactly parabolic (Fig. 3), and thus the dependence of the rate constant on ΔG^0 deviates somewhat from that predicted by the Marcus equation (*15*).

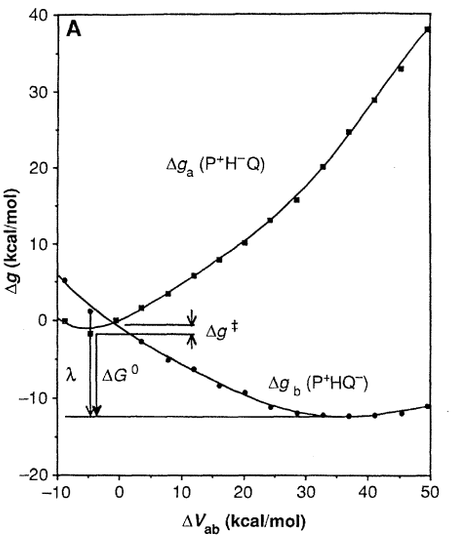

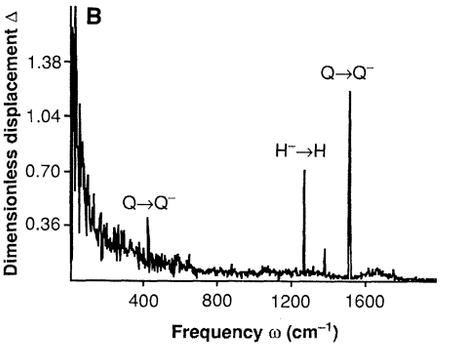

Fig. 3. (**A**) Calculated free energy surfaces for H^-Q (state a) and HQ^- (state b) in the *Rps. viridis* reaction center. The abscissa is the energy gap between the two states, ΔV_{ab}, which is taken as the reaction coordinate for the a → b reaction. The figure provides a microscopic estimate of the free energy difference between the two states (ΔG^0) and the reorganization energy (λ). The activation energy ($\Delta g^{\ddagger}$) is close to zero. (**B**) The dimensionless displacement $\Delta(\omega)$ obtained from the time-dependent energy gap of Fig. 1. The $\Delta(\omega)$ values are normalized by Eq. 4 and can be used in Eq. 3 by taking the values of Δ at equally spaced values of ω. Intramolecular vibrational modes that make the largest contributions in the $H^-Q \rightarrow HQ^-$ reaction are labeled "Q → Q⁻" and "H⁻ → H."

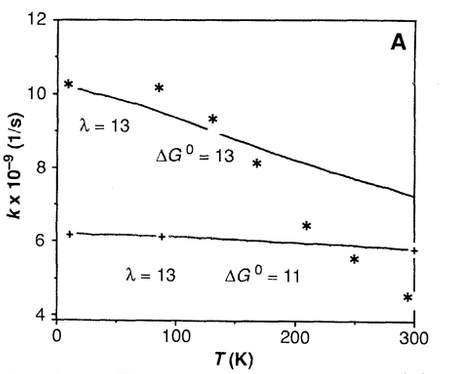

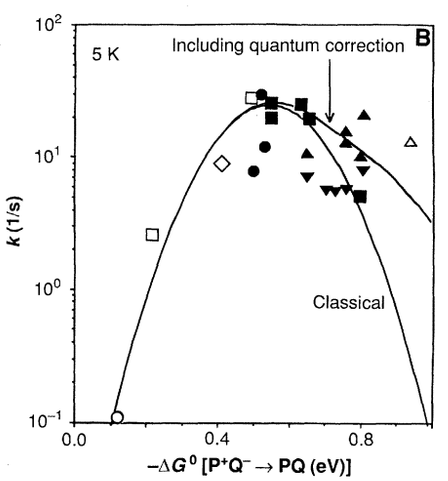

Fig. 4. (**A**) The temperature dependence of the rate constant for the $H^-Q \rightarrow HQ^-$ reaction, calculated with λ = 13 kcal/mol and ΔG^0 = 11 or 13 kcal/mol. Experimental results (*6*) are shown for reaction centers from *Rps. viridis* (+) and *Rb. sphaeroides* (*). The two sets of calculations (solid curves) are based on the *Rps. viridis* simulations but are done with different free energies. (**B**) The dependence of the rate constant on ΔG^0 for the back-reaction $P^+Q^- \rightarrow PQ$ at 5 K. The figure compares the calculated dependence to the results obtained experimentally (*8*) by varying the chemical nature of Q. (The different symbols represent various quinones.) The lower curve was obtained with the Marcus expression, which neglects nuclear tunneling; the upper curve was obtained with the treatment described in the text.

The λ from the free energy perturbation calculations was used with Eq. 4 to scale the Δ(ω) of Fig. 3B (*13, 18, 20*). Using Eq. 2, Δ(ω), and ΔG^0, we then calculated the temperature dependence of the $H^-Q \rightarrow HQ^-$ rate constant. The electronic coupling matrix element σ was adjusted to normalize the calculated and observed rate constants at 10 K. Because the calculated ΔG^0 is subject to an error of several kilocalories per mole (*4*), we used a range of values for the free energy change (Fig. 4A). [Experimental estimates of ΔG^0 for ET between H^- and Q vary considerably (*7, 21*), possibly because time-dependent relaxations can occur after the formation of P^+H^-.] The calculated temperature dependences encompass those seen experimentally, indicating that the QM nuclear tunneling effects can be reproduced by microscopic simulations that are based on the actual protein structure.

The most pronounced tunneling effect on ET occurs in the inverted region where ΔG^0 is negative and $|\Delta G^0| >> \lambda$. Such an effect is apparent in the back-reaction $P^+Q^- \rightarrow PQ$ at very low temperature (*7, 8*). Whereas the classical theory predicts that the rate of the reaction would depend strongly on ΔG^0 in this region, the experimentally measured rate is relatively insensitive to ΔG^0. The calculated QM rate constant (Fig. 4B) appears to reproduce the experimental data in a reasonable way, showing a significant deviation from the classical behavior in the inverted region. The difference between the classical and QM rate constant in the inverted region appears to be associated largely with the intramolecular $Q^- \rightarrow Q$ Franck-Condon factors.

The free energy perturbation treatment appears to provide a reasonably accurate quantitative estimate of the reorganization energy for the back-reaction, as can be judged by comparing the calculated and observed dependence of the rate constant on ΔG^0 (Fig. 4B). This is significant because the major experimental approach to exploring the relation between the rate constant and ΔG^0 for this reaction has involved chemical substitutions of other quinones in place of the native ubiquinone or menaquinone (*7*). A shortcoming of that approach is that each individual quinone could have its own characteristic vibrational frequencies and reorganization energies, making the use of a single phenomonological parameter for λ questionable. Furthermore, the primary steps in the photosynthetic charge-separation process could involve ET pathways for which the reorganization energies cannot be estimated from the available experimental information (*4*). The ability to calculate λ in a quantitative way could reduce the number of free parameters and should help in elucidating the actual mechanism of the charge-separation process.

The importance of intramolecular vibronic transitions in opening alternative channels for ET has been recognized in previous discussions of this and related systems (*6, 7, 10–13*), and an earlier calculation of the $P^+H^- \rightarrow PH$ back-reaction (*11*) indicated that the QM corrections could be very large. However, our microscopic approach does not single out a particular vibrational mode of the protein near 120 cm^{-1}, as has been suggested by the previous phenomonological analyses (*8, 10*), but rather points to the importance of numerous low-frequency protein modes. One of the many polarization modes that contribute to ET from H^- to Q is illustrated in Fig. 5. The protein microenvironment appears to control the rate constant by delocalized electrostatic effects rather than by one specific normal mode.

The finding that many protein modes are coupled to ET in the reaction center could help to explain why the primary charge-separation process is so efficient. One could view the relevant potential surfaces as consisting of many parallel parabolas rather than a single parabola. Having many small Franck-Condon factors at different frequencies should make the system insensitive to small perturbations.

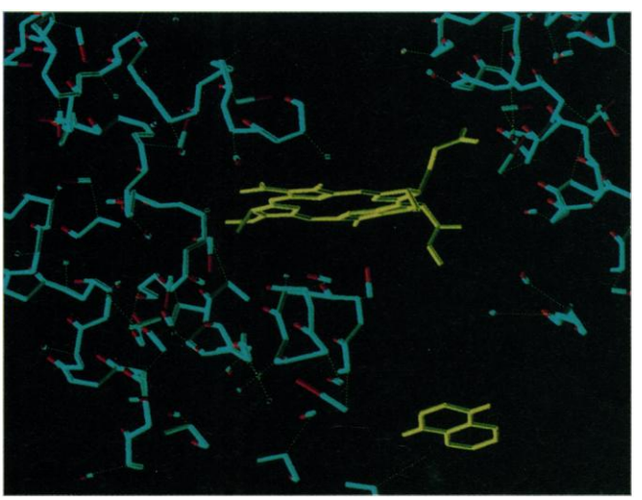

Fig. 5. One of the many polarization modes of the protein with a significant Franck-Condon factor for the $H^-Q \rightarrow HQ^-$ reaction. In order to monitor this mode, we added to the potential surface of H^- an oscillating electrostatic potential $\Delta V(\omega) = (V^b_{el} - V^a_{el})\cos(\omega_0 t) = \mathbf{E}\boldsymbol{\mu}_{a \rightarrow b}\cos\omega_0 t$, where $\omega_0^{-1} = 0.06$ ps (which corresponds to a frequency of 88 cm^{-1} in the power spectrum of Fig. 3), $\boldsymbol{\mu}_{a \rightarrow b}$ is the dipole moment associated with a transfer of an electron from H to Q, and **E** is the field from the protein on this dipole. The response of the protein trajectories to this potential can be approximated by the linear response theory [see (*22*) for a related treatment], and the polarization mode (or modes) with $\omega = \omega_0$ should follow the oscillating dipole. Thus, we evaluated the displacement vector of this mode by

$$\Delta\mathbf{r}(\omega_0) = [\sum_{j=1}^{n} \mathbf{r}(t_j) - \langle \mathbf{r} \rangle]/n$$

where $\omega_0 t_j = 2\pi j$. This multidimensional vector is depicted here in terms of the corresponding displacements of the side-chain dipoles ($\Delta\boldsymbol{\mu}_j = \Sigma_i \Delta\mathbf{r}_i q_i$), which are described by red arrows from the center of corresponding side chains. The vectors associated with the displacement of the main-chain amide dipoles are also described. The electron carriers H and Q are drawn in yellow.

REFERENCES AND NOTES

1. J. Deisenhofer, O. Epp, K. Miki, R. Huber, H. Michel, *Nature* **318**, 618 (1985); H. Michel, O. Epp, J. Deisenhofer, *EMBO J.* **5**, 246 (1986); J. Deisenhofer and H. Michel, in *Photosynthetic Bacterial Reaction Centers: Structure and Dynamics*, J. Breton and A. Vermeglio, Eds. (Plenum, New York, 1988), pp. 1–3.
2. C.-H. Chang *et al.*, *FEBS Lett.* **205**, 82 (1986).
3. J. P. Allen *et al.*, *Proc. Natl. Acad. Sci. U.S.A.* **84**, 5730 (1987).
4. S. Creighton, J.-K. Hwang, A. Warshel, W. W. Parson, J. Norris, *Biochemistry* **27**, 774 (1988).
5. W. W. Parson, *Biochim. Biophys. Acta* **131**, 154 (1966)
6. C. Kirmaier, D. Holten, W. W. Parson, *ibid.* **810**, 33 (1985); C. Kirmaier and D. Holten, in *Photosynthetic Bacterial Reaction Centers: Structure and Dynamics*, J. Breton and A. Vermeglio, Eds. (Plenum, New York, 1988), pp. 219–228.
7. N. W. Woodbury, W. W. Parson, M. R. Gunner, R. C. Prince, P. L. Dutton, *Biochim. Biophys. Acta* **851**, 6 (1986); R. J. Shopes and C. A. Wraight, *ibid.* **893**, 409 (1987).
8. M. R. Gunner, D. E. Robertson, P. L. Dutton, *J. Phys. Chem.* **90**, 3183 (1986); M. R. Gunner and P. L. Dutton, *J. Am. Chem. Soc.* **111**, 3400 (1989).
9. A. Gopher, Y. Blatt, M. Schonfeld, M. Y. Okamura, G. Feher, *Biophys. J.* **48**, 311 (1985); D. Kleinfeld, M. Y. Okamura, G. Feher, *ibid.*, p. 849.
10. D. DeVault, *Q. Rev. Biophys.* **13**, 387 (1980); R. A. Marcus and N. Sutin, *Biochim. Biophys. Acta* **811**, 265 (1985); M. D. Newton and N. Sutin, *Annu. Rev. Phys. Chem.* **35**, 437 (1984); M. Bixon and J. Jortner, *Faraday Discuss. Chem. Soc.* **74**, 17 (1982); W. Bialek and J. N. Onuchic, *Proc. Natl. Acad. Sci. U.S.A.* **85**, 5908 (1988).
11. A. Warshel, *Proc. Natl. Acad. Sci. U.S.A.* **77**, 3105 (1980).
12. ———, *J. Phys. Chem.* **8**, 2218 (1982); J.-K. Hwang and A. Warshel, *J. Am. Chem. Soc.* **109**, 715 (1987).
13. A. Warshel and J.-K. Hwang, *J. Chem. Phys.* **84**, 4938 (1986); Z. T. Chu, A. Warshel, W. W. Parson, *Photosynth. Res.*, in press.
14. An electron moving with the accompanying distortion of the medium is sometimes called a polaron. The medium vibrations (the phonons) are frequently treated with a single effective frequency (and sometimes a continuum of wave vectors). The term "dispersed polaron" was introduced to emphasize the treatment of the entire frequency spectrum of the phonons by means of a microscopic approach.
15. R. A. Marcus, *J. Chem. Phys.* **24**, 966 (1956).
16. An attempt to monitor $\Delta V(t)$ during a molecular

dynamics simulation was reported recently by H. Treutlein *et al.* [in *Photosynthetic Bacterial Reaction Centers: Structure and Dynamics*, J. Breton and A. Vermeglio, Eds. (Plenum, New York, 1988), p. 139]. However, the calculated ΔV did not reflect the relevant electrostatic energy and no rate constant was calculated.

17. R. Kubo and Y. Toyozawa, *Prog. Theor. Phys.* **13**, 160 (1955); S. H. Lin, *Theor. Chim. Acta* **10**, 301 (1968).
18. The dispersed polaron model is valid beyond the range of simple harmonic systems. Equation 4 reflects a quasi-harmonic approximation that uses harmonic wave functions as a basis set for anharmonic systems, by adjusting the harmonic frequencies according to a varitaion principle. [For a related treatment, see R. A. Friesner and R. M. Levy, *J. Chem. Phys.* **80**, 4488 (1984).] The present approach ensures that the intersection of V_a and V_b corresponds to the classical anharmonic activation energy, $\Delta g^{\ddagger}$. One could improve this approximation by an explicit consideration of the fact that both $\Delta g^{\ddagger}$ and λ are functions of temperature.
19. The use of ΔG^0 in Eq. 4 (rather than the potential difference between the minima of state a and state b) is particularly important in simulations of reactions with high activation barriers at high temperatures (*12, 13*). In simulations of fast relaxation processes such as the reaction $H^-Q \rightarrow HQ^-$, one really needs the value of $\langle \Delta V_{ba} \rangle_a$. This value requires long dynamics trajectories and a reliable estimate of the gas-phase free energy change (the α^i of Eq. 5). However, ΔG^0 and λ can be used in an approximate way to obtain $\langle \Delta V_{ba} \rangle_a$. In fact, one expects $\langle \Delta V_{ba} \rangle_a$ to change with time in a temperature-dependent manner as the system relaxes after the electron transfer [see (*21*) for related experimental information on the H^-Q system]. Such relaxations could be studied by direct simulations, but these would have to be longer than the one considered here.
20. The potential parameters used in Eq. 4 were the same as those used previously (*4*). We also evaluated the intramolecular gas-phase energy of forming HQ^- from H^-Q at infinite separation ($\alpha^b - \alpha^a$), following the approach described in (*4*). The starting coordinates for the calculations were taken from the x-ray structure (*1*) of *Rps. viridis* and included the atoms of P, H, and Q, the non-heme iron, and all amino acid residues within 18 Å of the electron D or A (either H and Q or Q and P, depending on the reaction). The calculations also allowed water molecules to fill any cavities within this region of the protein (*4*). All potentially ionizable amino acid residues were taken to be in their neutral forms; as argued by A. Warshel and S. Russell [*Q. Rev. Biophys.* **17**, 283 (1984)], the effective dielectric constant for ionized groups in proteins is large. The atomic charges for the electron carriers in their initial and final states were evaluated by the QM Consistent Force Field for π electron systems (QCFF/PI) method with the parameters taken from the following: A. Warshel and A. Lappicirella, *J. Am. Chem. Soc.* **103**, 4464 (1981); A. Warshel and W. W. Parson, *ibid.* **109**, 6143 (1987). We obtained the intramolecular potential surface V^i_{strain} by using a classical force field that approximated the corresponding QCFF/PI surface, representing the change of the potential between different redox states in terms of shifted harmonic potentials. [Intramolecular Franck-Condon factors for these shifted surfaces have been evaluated (*11, 12*).] The non-heme iron atom, which is well solvated by nearby glutamic acid and histidine residues, was assigned an effective charge of +0.2. The region of the protein that was treated in detail was assumed to be surrounded by a continuum with a dielectric constant of 2 to represent the membrane and the rest of the protein.

    The calculations were done by the program ENZYMIX, running a 20-ps trajectory at 300 K on V_a and recording the energy gap $\Delta V_{ba}(t) = V_b(t) - V_a(t)$ for the last 10 ps. (During the first few picoseconds, the molecular structure relaxes very rapidly toward an energy minimum for the state P^+H^-. This initial relaxation probably is not relevant to the $H^-Q \rightarrow HQ^-$ reaction, which occurs on the time scale of 200 ps.) The time-dependent energy gap during the second period (Fig. 1) was used to obtain the frequency-dependent origin shifts, $\Delta(\omega)$, of Fig. 4 by a Fourier transform procedure (*13*).
21. V. A. Shuvalov, I. N. Krakhmaleva, V. V. Klimov, *Biochim. Biophys. Acta* **449**, 597 (1976); A. W. Rutherford, P. Heathcote, M. C. W. Evans, *Biochem. J.* **182**, 515 (1979); R. C. Prince, J. S. Leigh, P. L. Dutton, *Biochim. Biophys. Acta* **440**, 622 (1976); N. W. Woodbury and W. W. Parson, *ibid.* **767**, 345 (1984); J. K. H. Horber, W. Gobel, A. Ogrodnik, M. E. Michel-Beyerle, R. J. Cogdell, *FEBS Lett.* **198**, 273 (1986).
22. J.-K. Hwang *et al.*, *J. Chem. Phys.* **89**, 859 (1988).
23. Supported under NIH grant GM-40283 and NSF grant PCM-8616161. We thank J. Deisenhofer for providing the crystallographic coordinates of the reaction center.

15 May 1989; accepted 8 August 1989

Symbiotic Marine Bacteria Chemically Defend Crustacean Embryos from a Pathogenic Fungus

M. SOFIA GIL-TURNES, MARK E. HAY, WILLIAM FENICAL

Embryos of the shrimp *Palaemon macrodactylus* are remarkably resistant to infection by the fungus *Lagenidium callinectes*, a recognized pathogen of many crustaceans. An *Alteromonas* sp. bacterial strain consistently isolated from the surface of the embryos, produces 2,3-indolinedione (isatin), a compound that inhibits the pathogenic fungus. If exposed to the fungus, bacteria-free embryos quickly die, whereas similar embryos reinoculated with the bacteria or treated only with 2,3-indolinedione live well. The commensal *Alteromonas* sp. bacteria protect shrimp embryos from fungal infection by producing and liberating the antifungal metabolite 2,3-indolinedione.

THE PRODUCTION OF SECONDARY metabolites, or allelochemicals (*1*), by microbes is thought to be an important adaptation allowing microbes to affect their hosts, competitors, and predators (*2–4*). However, it is difficult to extrapolate laboratory experiments to the complex interactions of microbes in nature (*5*) and few rigorous tests of these ideas have been conducted with ecologically relevant organisms. Thus, the chemical ecology of microorganisms has remained a largely hypothetical field (*6*), and one in need of new research approaches to confirm the natural functions of microbial metabolites.

Many organisms remain free of pathogenic fungi and bacteria as long as they retain a specific group of microorganisms that constitute normal associated flora (*7–9*) on their surface. In some instances, epibiotic microorganisms produce compounds that inhibit competing microorganisms (*10–12*). It has been suggested that commensal microorganisms may chemically defend their microhabitat, thus providing their host protection from pathogenic microorganisms (*13, 14*). Our research confirms that antimicrobial compounds produced by marine bacteria are important in microbial competition and host viability.

Although juveniles and larvae of the caridean shrimp *Palaemon macrodactylus* are highly vulnerable to infection by the phycomycetous fungus *Lagenidium callinectes* (*15*) [a pathogen of many crustaceans (*16–18*)], externally brooded embryos of are remarkably resistant to the fungus. Fisher (*19*) isolated several bacterial strains from the surface of healthy *P. macrodactylus* embryos and noted that the embryos were quickly colonized by a variety of different microorganisms when their associated bacteria were removed by treatment with penicillin. The fungus *L. callinectes* was one of the most frequent and vigorous pathogens (*20*), and infection always resulted in death. A penicillin-sensitive bacterial strain (culture I-2, an *Alteromonas* sp.) that is consistently isolated from healthy embryos was found to effectively inhibit the growth of the fungus *L. callinectes* in vitro. We found that this strain produces, and releases into the culture medium, relatively large quantities of an antifungal compound (*21*). We have isolated and identified this compound as 2,3-indolinedione (*22*) (also known as isatin), a substance previously known mainly as a synthetic intermediate in the production of indigo dyes, but known to possess significant pharmacological properties (*23*) (Fig. 1).

To confirm that the bacterial isolate protects the embryos from fungi and that protection is mediated by 2,3-indolinedione, we performed the following experiment on four groups of embryos. Clusters of embryos were detached from 20 different *P. macrodactylus* females. Each embryo cluster was divided in four groups of about 30 embryos each (*24*). The epibiotic bacteria were eliminated from three of these groups by treatment with penicillin-G (*25*). One group

M. S. Gil-Turnes and W. Fenical, Scripps Institution of Oceanography, University of California, San Diego, La Jolla, CA 92093-0228.
M. E. Hay, Institute of Marine Sciences, University of North Carolina at Chapel Hill, Morehead City, NC 28557.